

The Crystal Structure of *Leishmania major* 3-Mercaptopyruvate Sulfurtransferase

A THREE-DOMAIN ARCHITECTURE WITH A SERINE PROTEASE-LIKE TRIAD AT THE ACTIVE SITE*

Received for publication, July 5, 2003, and in revised form, August 26, 2003
Published, JBC Papers in Press, September 1, 2003, DOI 10.1074/jbc.M307187200

Magnus S. Alphey‡, Roderick A. M. Williams§, Jeremy C. Mottram¶, Graham H. Coombs§,
and William N. Hunter‡**

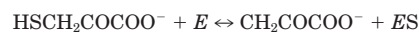
From the ‡Division of Biological Chemistry and Molecular Microbiology, School of Life Sciences, University of Dundee, Dundee DD1 5EH, the §Division of Infection and Immunity, Institute of Biomedical and Life Sciences, University of Glasgow, Glasgow G12 8QQ, and the ¶Wellcome Centre for Molecular Parasitology, Anderson College, University of Glasgow, 56 Dumbarton Road, Glasgow G11 6NU, Scotland, United Kingdom

***Leishmania major* 3-mercaptopyruvate sulfurtransferase is a crescent-shaped molecule comprising three domains. The N-terminal and central domains are similar to the thiosulfate sulfurtransferase rhodanese and create the active site containing a persulfated catalytic cysteine (Cys-253) and an inhibitory sulfite coordinated by Arg-74 and Arg-185. A serine protease-like triad, comprising Asp-61, His-75, and Ser-255, is near Cys-253 and represents a conserved feature that distinguishes 3-mercaptopyruvate sulfurtransferases from thiosulfate sulfurtransferases. During catalysis, Ser-255 may polarize the carbonyl group of 3-mercaptopyruvate to assist thiophilic attack, whereas Arg-74 and Arg-185 bind the carboxylate group. The enzyme hydrolyzes benzoyl-Arg-*p*-nitroanilide, an activity that is sensitive to the presence of the serine protease inhibitor *N*^α-*p*-tosyl-L-lysine chloromethyl ketone, which also lowers 3-mercaptopyruvate sulfurtransferase activity, presumably by interference with the contribution of Ser-255. The *L. major* 3-mercaptopyruvate sulfurtransferase is unusual with an 80-amino acid C-terminal domain, bearing remarkable structural similarity to the FK506-binding protein class of peptidylprolyl *cis/trans*-isomerase. This domain may be involved in mediating protein folding and sulfurtransferase-protein interactions.**

Sulfurtransferases (EC 2.8.1.1–5) catalyze the transfer of sulfane sulfur from a donor molecule to a thiophilic acceptor. These enzymes are widely distributed in plants, animals, and bacteria (1–3) and have been implicated in a wide range of biological processes. For example, sulfurtransferases may be involved in the formation and maintenance of iron-sulfur clusters in protein (4, 5), detoxification of cyanide (6, 7), degradation of cysteine (8), biosynthesis of the molybdopterin cofactor of xanthine oxidase (9), selenium metabolism (2, 10), and thiamine and 4-thiouridine biosynthesis (11, 12). The expression of specific sulfurtransferases is up-regulated under conditions of peroxide or hypo-sulfur stress, osmotic shock, and phage

infection (13), suggesting that such enzyme activity is protective of the cell and/or involved in repair processes. Nevertheless, despite intensive study, the biological functions and identification of the physiological substrates of sulfurtransferases remain uncertain.

The archetypal sulfurtransferase is rhodanese, a thiosulfate: cyanide sulfurtransferase (TST)¹ able to catalyze the transfer of the thiosulfate sulfur to cyanide *in vitro*. The related 3-mercaptopyruvate sulfurtransferase (3-mercaptopyruvate:cyanide sulfurtransferase (MST)), first discovered in rat liver (14), catalyzes reactions similar to those catalyzed by rhodanese, but uses 3-mercaptopyruvate in preference to thiosulfate as the donor in the two-step reaction,



STEP 1



STEP 2

where *E* represents the free enzyme and *ES* the enzyme-sulfur adduct.

Crystal structures of rhodanases have been elucidated and analyzed in detail (15–20). The enzyme consists of two domains that, despite a low level of sequence identity, are structurally homologous. Each domain, often referred to as a rhodanese domain, is constructed from a five-stranded β-sheet core surrounded by five α-helical sections. The active site, with a catalytic cysteine, is situated in a cleft formed at the interface of the domains, although it is mainly constructed from residues associated with the C-terminal domain. For that reason, this domain is often termed the active domain, whereas the N-terminal domain is described as inactive.

Rhodanese-related enzymes are composed of either two rhodanese domains or a single, catalytically active rhodanese domain (1, 21). The rhodanese-like domain has been observed in association with other protein domains, *e.g.* in mitogen-activated protein kinase phosphatases (22, 23). The similarity be-

* This work was supported by the Wellcome Trust and Commonwealth Office. The costs of publication of this article were defrayed in part by the payment of page charges. This article must therefore be hereby marked "advertisement" in accordance with 18 U.S.C. Section 1734 solely to indicate this fact.

¶ Medical Research Council (United Kingdom) Senior Research Fellow.

** Wellcome Trust Senior Research Fellow. To whom correspondence should be addressed. Tel.: 44-1382-34-5745; Fax: 44-1382-34-5764; E-mail: w.n.hunter@dundee.ac.uk.

¹ The abbreviations used are: TST, thiosulfate:cyanide sulfurtransferase; MST, 3-mercaptopyruvate:cyanide sulfurtransferase; *LmMST*, *L. major* 3-mercaptopyruvate:cyanide sulfurtransferase; *pNA*, *p*-nitroanilide; *SeMet*, selenomethionine; *BisTris* propane, 1,3-bis[tris(hydroxymethyl)methylamino]propane; *Bz*-, benzoyl-; *TLCK*, *N*^α-*p*-tosyl-L-lysine chloromethyl ketone; *TPCK*, tosylphenylalanyl chloromethyl ketone; *r.m.s.d.*, root mean square deviation; *FKBP*, FK506-binding protein; *MIP*, macrophage infectivity potentiator protein; *PPIase*, peptidylprolyl *cis/trans*-isomerase.

tween rhodanese and this phosphatase extends from the overall fold to spatial conservation of the active-site cysteine utilized by both enzymes. This suggests that the rhodanese fold is optimized for activation of a catalytic cysteine.

Although there is no structure yet available for any MSTs, several observations suggest that they are evolutionarily and structurally related to TSTs (1, 4, 6). The two types of enzyme catalyze the sulfurtransferase reaction via the formation of a persulfide sulfur covalently bound to the thiol of a catalytic cysteine and display significant levels of sequence similarity, and some are immunologically cross-reactive. However, the different preferred *in vitro* sulfur donors suggest that the enzymes have different *in vivo* substrates and physiological roles.

Despite the presence of a conserved catalytic cysteine, suggestive of a similar mechanism, the amino acid composition and location of charged residues in the active site of TSTs and MSTs are distinct (21). In TSTs, two large and basic residues within the hexapeptide motif Cys-Arg-Lys-Gly-Val-Thr follow the catalytic cysteine. In MSTs, the Arg-Lys pair is replaced by a Gly-Ser or Gly-Thr combination. Mutation of these particular residues to those observed in the other family of enzymes results in partial conversion to that activity, *i.e.* MST becomes more rhodanese-like and *vice versa* (24, 25). Studies on the sulfurtransferase SseA, an *Escherichia coli* protein involved in serine sensitivity, have reinforced the observation that the sequence following the active-site cysteine can distinguish sulfurtransferases as TSTs or MSTs (26), but the structural consequences of such non-conservative amino acid differences to the active site of MST were unclear.

Williams *et al.* (27) recently identified and characterized a cytosolic MST from the parasitic trypanosomatid *Leishmania major* (*LmMST*). Expression of this enzyme is up-regulated in *L. major* promastigotes during conditions of oxidative stress, suggesting an involvement in detoxification of peroxides; and, in common with *E. coli* and mammalian MSTs (28–30), *LmMST* is able to utilize thioredoxin as the thiophilic acceptor. It was also reported that *LmMST* can fold independently (27), in contrast to many other sulfurtransferases, which require molecular chaperones to assist such a process (31). It was hypothesized that the unusual 80-amino acid C-terminal extension in *LmMST* may play a part in the folding process, particularly as short truncations of this region resulted in misfolded protein (27).

The availability of a stable and active recombinant enzyme allowed us to initiate a crystallographic study to delineate structure-activity relationships in an MST with the aims of characterizing the active site, investigating the roles of the two residues immediately following the catalytic cysteine, determining the structure of the C-terminal extension, and providing an MST model for detailed comparisons with TSTs. A number of assays using peptidyl-*p*-nitroanilide (*pNA*) substrates were carried out seeking to identify additional enzyme activities.

MATERIALS AND METHODS

Sample Preparation and Crystallization—Recombinant *LmMST* was expressed and purified according to Williams *et al.* (27). Initial crystallization trials used the sparse matrix approach (32), applying the hanging drop vapor diffusion technique with reagents from Hampton Research. Crystals were grown overnight under Crystal Screen I condition 46 (18% (w/v) polyethylene glycol 8000, 100 mM sodium cacodylate (pH 6.5), and 200 mM calcium acetate) at 20 °C. Optimization of these conditions resulted in crystals with approximate dimensions of $0.3 \times 0.3 \times 0.2$ mm³ from a drop consisting of 1 μ l of protein (3.5 mg/ml) and 1 μ l of reservoir (14% (w/v) polyethylene glycol 8000, 80 mM sodium cacodylate (pH 6.5), and 160 mM calcium acetate). Crystals were cryoprotected with 20% glycerol and maintained at –170 °C for transportation to beamline ID29 at the European Synchrotron Radiation Facility (Grenoble, France), where data were measured.

Native crystals of *LmMST* diffracted to 2.7-Å resolution and display the tetragonal space group $P4_22_1$ with unit cell lengths of $a = 109.6$ and $c = 67.3$ Å. The asymmetric unit contains a single polypeptide with an approximate molecular mass of 42 kDa, a solvent content of ~49%, and $V_m = 2.4$ Å³/Da.

The methionine auxotrophic strain of *E. coli*, B834(DE3), was heat shock-transformed with the plasmid carrying the gene for *LmMST* (27) and selected on LB agar plates containing 100 μ g/ml ampicillin. Bacteria were cultured in M9 minimal medium containing selenomethionine (Se-Met). Expression of *LmMST* was induced at mid-log phase with 0.6 mM isopropyl- β -D-thiogalactopyranoside, and cell growth continued overnight. Cells were harvested by centrifugation at $2500 \times g$, resuspended in binding buffer (20 mM Tris-HCl (pH 7.5), 500 mM NaCl, 5 mM imidazole, and 5 mM benzamide) and, following the addition of deoxyribonuclease I and lysozyme, were lysed using a French press. Insoluble debris was separated by centrifugation at $27,000 \times g$ for 20 min at 4 °C, and the supernatant containing soluble *LmMST* was passed through a 0.2- μ m syringe filter and then applied to a Ni²⁺-resin column (HiTrap, Amersham Biosciences) pre-equilibrated with binding buffer. Following a wash with 20 mM BisTris propane and 10 mM imidazole (pH 7.5) using a BioCAD 700E (Applied Biosystems), the product was eluted with a linear imidazole gradient from 0 to 500 mM. Fractions were analyzed by SDS-PAGE, and those containing *LmMST* were pooled and dialyzed overnight against 20 mM Tris-HCl (pH 8.0) and 50 mM NaCl. The sample was then subjected to anion-exchange chromatography on a 5-ml Q-Sepharose column (Amersham Biosciences). The resin was washed with 25 mM BisTris propane (pH 8.0), and MST was found in the flow-through and wash fractions. These fractions were passed over a second Ni²⁺-resin column to concentrate the protein, and *LmMST* was eluted with a linear imidazole gradient from 0 to 500 mM. Fractions containing *LmMST* were again pooled and dialyzed overnight in 20 mM Tris-HCl (pH 8.0) and 50 mM Na₂S₂O₃. The dialyzed protein was concentrated (Centricon-10/Microcon-10, Millipore Corp.) to ~3.5 mg/ml for use in crystallization experiments. SDS-PAGE and matrix-assisted laser desorption/ionization time-of-flight mass spectrometry were used to assess purity, and the latter technique was also used to confirm full incorporation of 12 SeMet residues. Crystals of the SeMet MST protein grew under the same conditions as, and are isomorphous with, the native crystals, but diffracted to higher resolution.

Data Collection and Processing—Data were measured at the European Synchrotron Radiation Facility (beamline ID14 EH2). A single SeMet derivative crystal was soaked in a solution of 70% reservoir and 30% glycerol for 10 s and flash-cooled in a stream of nitrogen gas at –170 °C. The wavelength used was 0.933 Å, and a highly redundant data set (180 \times 1° oscillations; Data set 1) was measured on an ADSC Quantum4 detector, processed, and scaled using the HKL suite of programs (33). Processing statistics are presented in Table I.

Single Wavelength Anomalous Dispersion Phasing, Structure Solution, Model Building, and Refinement—Ten selenium positions were identified using the program SOLVE (34) and used for phase calculation, giving a figure of merit of 0.23 to 2.1-Å resolution (MLPHARE) (35). The first electron density maps were of poor quality, but density modification and histogram matching with the program DM (36) were spectacularly successful and increased the figure of merit to 0.76. The programs ARPwARP (37) and MAID (38) were used to construct sections of the polypeptide backbone into this map. In addition, MOLREP (39) positioned a polyaniline model of bovine rhodanese (Protein Data Bank code 1ORB) (16) into the experimentally phased map. The results from all of these programs were combined to produce a polyaniline model of *LmMST* onto which side chains were assigned using O (40). A subset of data (5%) was set aside for the calculation of R_{free} (41) and used as a guide for the refinement. The Hendrickson-Lattman coefficients derived from the DM calculations were included as phase restraints in the early stages of refinement. Several rounds of refinement with CNS (crystallography and NMR system) (42) and REFMAC5 (43) interspersed with rounds of model building produced a model for *LmMST*. The electron and difference density maps were noisy, especially at the selenium positions, and the highly redundant data set displayed evidence of radiation damage; so a truncated data set based on the first 70° of data was prepared and used to complete the refinement (Data set 2) (see Table I). Further refinement with the addition of water molecules and ions completed the analysis. Residues 1–6 and 239–243 are disordered. The stereochemistry of the model was assessed with PROCHECK (see Table I for details) (44), and secondary structure was assigned using PROMOTIF (45).

Enzyme Assays—The serine protease activity of *LmMST* was assayed with various peptidyl-*pNA* substrates (benzoyl (Bz)-Pro-Phe-Arg-*pNA*, Bz-Phe-Val-Arg-*pNA*, Bz-Arg-Arg-*pNA*, and Bz-Arg-*pNA*, each dissolved in dimethyl sulfoxide) in a reaction mixture of 100 mM Tris-HCl

TABLE I
Data processing and refined model statistics

Numbers in parentheses correspond to the highest resolution shell, a bin of 2.17 to 2.10 Å. $R_{\text{sym}} = \sum |I - \langle I \rangle| / \sum I$, where the summation is over all symmetry equivalent reflections. $R_{\text{anom}} = \sum |I(+)-I(-)| / \sum (I(+)+I(-))/2$.

	Data set 1	Data set 2
Resolution range (Å)	20-2.10	20-2.10
No. reflections	348,345	131,345
No. unique reflections	24,450	23,924
Redundancy	14.2	5.4
Wilson B (Å ²)	35.8	36.1
Completeness (%)	99.9 (99.3)	97.8 (97.2)
$I/\sigma I$	42.1 (7.8)	23.2 (4.5)
R_{sym} (%)	5.1 (28.2)	4.7 (31.6)
R_{anom} (%)	1.9	
Protein residues/atoms		360/2786
Water molecules/ions		407/SO ₃ ²⁻ , AsO ₃ ²⁻ , Ca ²⁺
R_{work} (%) / No. observations		20.8 (23.4) / 22691 (1632)
R_{free} (%) / No. observations		28.7 (30.5) / 1225 (67)
Average isotropic thermal parameters		(Å ²)
Overall/main chain/side chain		41.3/40.7/41.9
Waters/SO ₃ ²⁻ /Ca ²⁺		54.4/56.9/65.0
r.m.s. bond lengths (Å) / angles		0.016/1.7°
r.m.s. planarity (Å) / G factor		0.007/-0.1
Ramachandran analysis		
Favorable (%)		81.6
Additionally favorable (%)		16.4
Acceptable (%)		2.0

(pH 8.0), 10 mM β-mercaptoethanol, and 75 μg of *LmMST*. The reaction was started by the addition of *pNA* substrate diluted to a final concentration of 3 mM in the assay mixture at 37 °C and was monitored continuously for 30 min by detecting the release of *pNA* spectrometrically at 420 nm. The molar extinction coefficient was taken as $9.5 \times 10^3 \text{ cm}^{-1} \text{ M}^{-1}$. Trypsin (Promega) was used as the control. Sulfurtransferase activity was measured using 3-mercaptopyruvate as substrate and lead acetate to trap the H₂S released (27). Inhibition of these activities was assayed following a 30-min preincubation of *LmMST* at 37 °C in 100 mM Tris-HCl (pH 8.0) containing the appropriate concentration of the following inhibitors: phenylmethanesulfonyl fluoride (0.1–5 mM), TLCK (7–400 μM), TPCK (10–100 μM), and E-64 (*L-trans*-epoxysuccinyl-L-leucylamido-(4-guanidino)butane; 1–50 μM).

RESULTS AND DISCUSSION

Structure Determination—Recombinant *LmMST* has been cloned, expressed, and purified, and ordered crystals (diffracting to 2.7-Å resolution) have been obtained and characterized. The crystals are tetragonal and display space group $P4_22_12$ with $a = 109.6$ and $c = 67.3$ Å, and the asymmetric unit contains a single polypeptide. Attempts to solve the structure by molecular replacement were unsuccessful; therefore, experimental phase information was sought from a SeMet derivative. The SeMet *LmMST* crystallized isomorphously and provided improved diffraction to 2.1-Å resolution (Table I). Initial phase information was obtained using a single wavelength anomalous dispersion approach with a highly redundant (oscillation range of 180°) data set. Density modification produced an electron density map (Fig. 1) into which the molecular model was constructed, and then refinement was initiated. Because of the effects of radiation damage, a modified data set (the first 70° of oscillation data) was used to complete the refinement. A sulfite is bound in the active site, and the catalytic Cys-253 is persulfurated, likely consequences of the Na₂S₂O₃ that was included during the enzyme purification and in the protein solutions from which crystals were grown. Cys-331 is also persulfurated; Cys-80 appears as an arsenocysteine, a consequence of the crystallization conditions containing cacodylate,

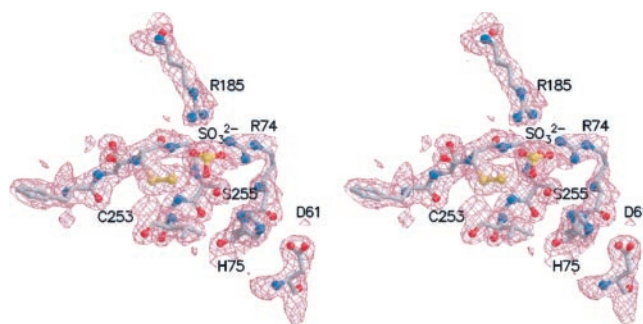


FIG. 1. Stereo view of the electron density map after density modification (salmon pink) contoured at the 1σ level around selected residues of the active site. The refined model is shown in ball-and-stick format, colored blue for nitrogen, gray for carbon, red for oxygen, and yellow for sulfur atoms.

and has been modeled in two orientations, each of occupancy 0.5 (see Table I for further details).

Shape, Fold, and Secondary Structure—Monomeric *LmMST* is a crescent-shaped molecule with approximate dimensions of $70 \times 50 \times 40$ Å (Fig. 2*a*) and comprising N-terminal, central, and C-terminal domains. The N-terminal domain of ~160 residues exhibits the rhodanese-like domain fold with a five-stranded parallel β-sheet (β1, β2, β4, β5, and β6) surrounded by five α-helices (α1–α5) and a small section of 3₁₀-helix (θ1) (Fig. 2, *a* and *b*). In addition, a two-stranded antiparallel β-sheet (β3 and β7) is placed on one side of the parallel β-sheet. The N-terminal domain is connected to the central domain via an extended section of polypeptide on the outer surface of the protein. The central domain (residues 167–288) also exhibits a rhodanese-like fold, this time a four-stranded parallel β-sheet (β8, β9, β12, and β13) surrounded by four α-helices (α6–α9) and two small sections of 3₁₀-helix (θ2 and θ3). A small two-stranded antiparallel β-sheet (β10 and β11) is also present in this domain. The sulfurtransferase active site is positioned between the two rhodanese-like domains and is described below. Two proline residues (positions 290 and 291) produce an ~90° bend between helices α9 and α10. Helix α9 completes the central domain, and helix α10 represents the start of the C-terminal domain (residues 290–370). This third domain comprises a four-stranded antiparallel β-sheet (β14, β15, β16, and β17) with an α-helix (α11) between strands β15 and β16 and an extended loop between strands β14 and β15 (Fig. 2, *a* and *b*).

The Rhodanese Domains—Twenty-one MST amino acid sequences and seven rhodanese sequences were retrieved from EXPASY² and aligned with the *LmMST* sequence with ClustalW (data not shown) (46). The overall sequence identity within the MST family is only ~20%, although higher values are observed when comparing the MSTs of trypanosomatids (27): *L. major* and *Leishmania mexicana* (95%) and *L. major* and *Trypanosoma brucei* (45%). The conservation of amino acid residues is pronounced in and around the active site and at the core of the rhodanese-like domains. The active-site Cys-Gly-Ser-Gly-Val-(Thr/Ser) motif (residues 253–258 in *LmMST*) is strictly conserved in all MSTs. The alignment of *LmMST* with rhodanases revealed that ~18% of the residues are strictly conserved and that the rhodanases themselves exhibit a sequence identity level ranging from 30 to 95%.

The coordinates of the N-terminal and central domains of *LmMST* were submitted to the DALI server (47) to compare with those in the Protein Data Bank (48). A close structural relationship was observed with bovine rhodanese (Protein Data Bank code 1RHS) (15). The sequence identity of the two en-

² Available at ca.expasy.org.

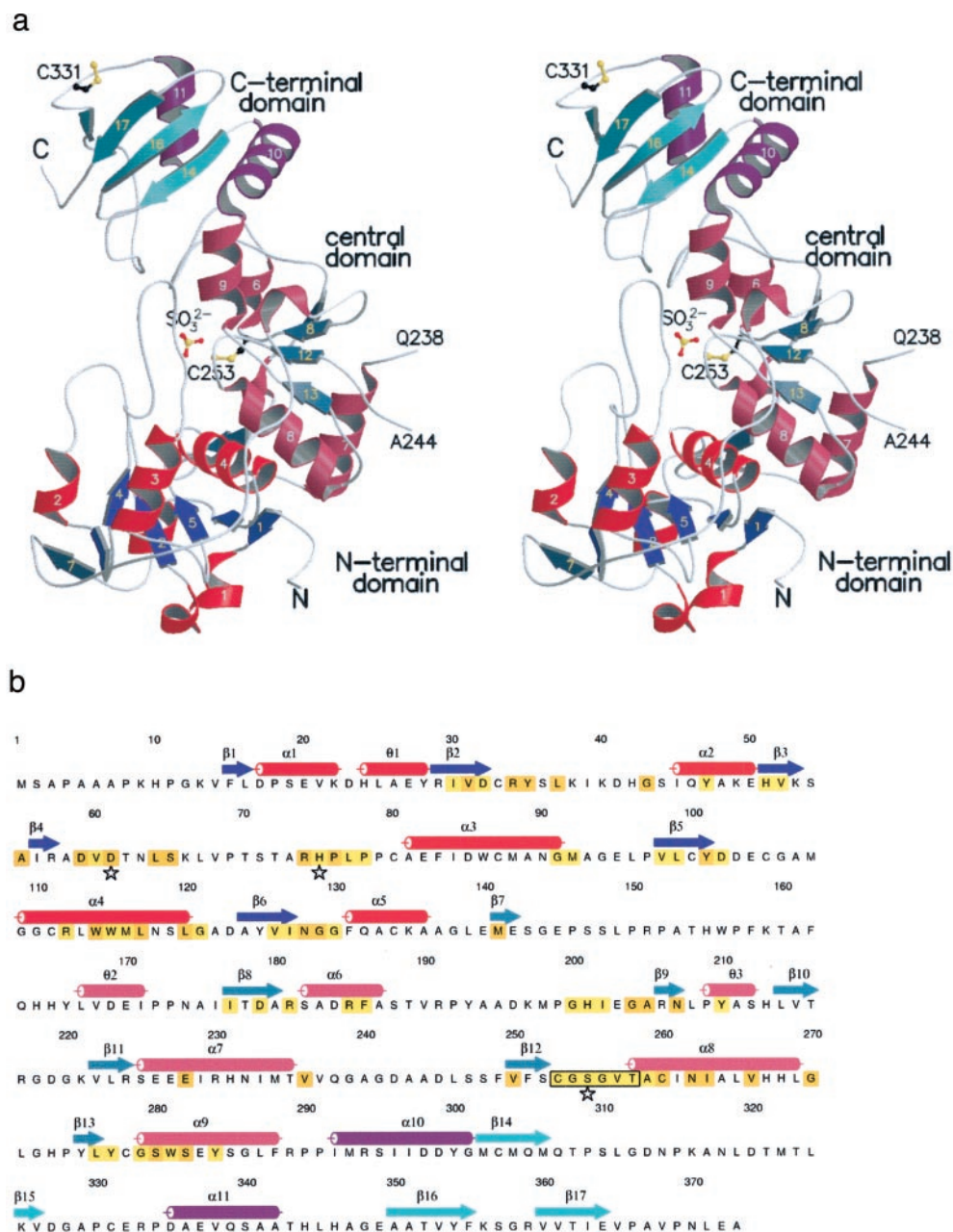


FIG. 2. *a*, stereo view ribbon diagram of *LmMST*. The inactive N-terminal, central, and C-terminal domains are labeled, and the secondary structure associated with each is colored navy blue and red, slate blue and maroon, and cyan and magenta, respectively. The sulfite binding in the active site and the persulfurated cysteines in the active site (Cys-253) and C-terminal domain (Cys-331) are depicted in ball-and-stick representation. Helices are numbered in white, and strands in yellow. The loop between Gln-238 and Ala-244 is disordered. Figs. 2*a*, 3, 4, and 6 were prepared using MOLSCRIPT (63). *b*, amino acid sequence and secondary structure of *LmMST*. β -Strands are depicted by arrows, and α -helices and 3_{10} -helices (θ) by cylinders, and are colored as described for *a*. The active-site hexapeptide sequence is boxed. Residues strictly conserved in the MST family (see "Results and Discussion") are highlighted in yellow, whereas homologous residues are highlighted in orange. Stars indicate the three residues composing the active-site serine protease-like triad. This figure was prepared using ALINE (C. S. Bond, personal communication).

zymes is 23%, and an overlay gives a root mean square deviation (r.m.s.d.) of 2.4 Å for 267 C- α pairs and a Z-score of 29.6. The Z-score is a measure of the statistical significance of the best alignment determined in DALI; and, typically, two dissimilar proteins have a Z-score of ≤ 2 . MST matched against itself with a Z-score of 57. The DALI superposition was optimized using the graphics program O, and the r.m.s.d. was reduced to 1.7 Å for 224 C- α pairs. This is the superposition shown in Fig. 3*a*. Two other homologs of note were identified. First, *E. coli* GlpE (Protein Data Bank code 1GN0) (21), which shares a sequence identity of 22% with the central domain of *LmMST*, gives an r.m.s.d. of 2.5 Å over 101 C- α atoms and a Z-score of 11.0. This protein is encoded by a gene on the *sn*-glycerol

3-phosphate regulon (*glp*) and is a single domain rhodanese-type sulfurtransferase. Second, the catalytic domain of human CDC25A phosphatase (Protein Data Bank code 1C25) (22), which shares a sequence identity of 22% with *LmMST*, produces an r.m.s.d. of 2.4 Å over 97 C- α pairs and a Z-score of 8.2. Despite only limited sequence conservation between these distinct enzyme families, the structural overlays indicate that secondary structure is well conserved, with large-scale structural differences restricted to surface loops.

Although only 12% identical in amino acid sequence, superposition of the N-terminal and central domains of *LmMST* gives an r.m.s.d. of 2.0 Å for 104 C- α pairs (Fig. 3*b*). This compares favorably with the superposition of the two domains

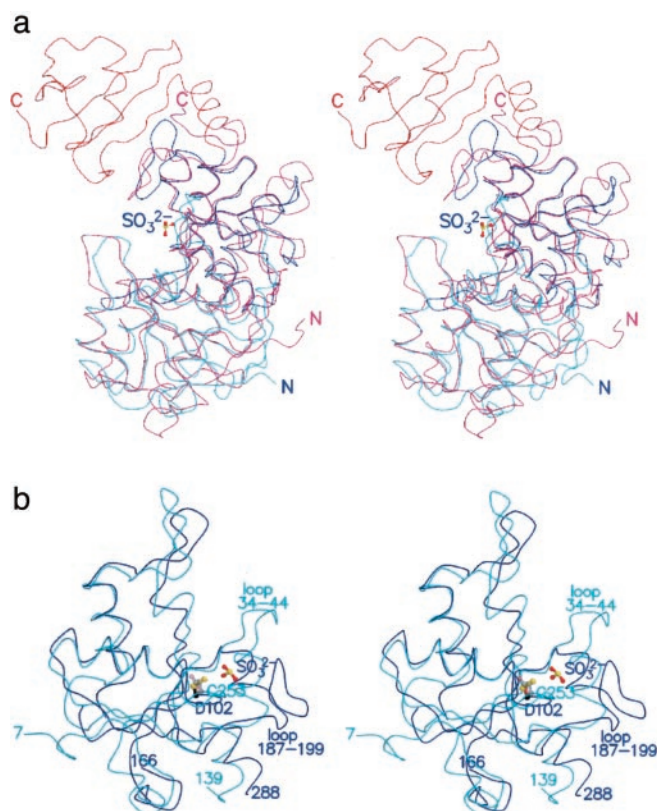


FIG. 3. *a*, stereo view depicting superposition of C- α traces of *LmMST* (red) and bovine rhodanese (Protein Data Bank code 1RHS). The N-terminal domain of *LmMST* is cyan; the central domain is blue; and the C-terminal domain is red. The trace for rhodanese is magenta. The view is the same as in Fig. 2*a*. *b*, stereo view of the two rhodanese-like domains of *LmMST* superimposed. The N-terminal domain is colored cyan, and the central domain is blue. The active-site Cys-253 and the spatially equivalent N-terminal Asp-102 are included.

from bovine rhodanese, which gives an r.m.s.d. of 1.6 Å over 114 C- α atoms. As with the comparisons described above, the elements of secondary structure of each *LmMST* domain are conserved, and differences occur in the loops. The loop formed by residues 34–44 in the N-terminal domain is absent from the central domain; and, conversely, the loop formed by residues 187–199 in the central domain is not present in the N-terminal domain. This latter loop segment provides a number of side chains that protrude into the active site and also supplies one partner for a salt bridge (Arg-191 with Glu-349) that serves to link the central domain to the C-terminal domain (data not shown).

The residue in the N-terminal domain of *LmMST* that occupies the equivalent position of the central domain active-site Cys-253 is Asp-102 (Fig. 3*b*). The acidic side chain of Asp-102 participates in six hydrogen bonding interactions with the main chain amide groups of residues 103, 104, 106, and 108–110 and is unavailable for substrate or ion binding. A similar observation has been described for rhodanese (19).

The C-terminal Domain—The *L. major*, *L. mexicana*, and *T. brucei* MST sequences differ from other family members with an extension of ~80 residues (27). These extensions display a high level of sequence conservation (41% identity plus a further 10% similarity) and form a distinctive C-terminal domain appended onto the tandem repeat of rhodanese domains. The function of the C-terminal domain is uncertain; therefore, clues were sought from an architectural comparison in DALI. This identified structural homology to specific domains of the immunosuppressant FK506-binding protein (FKBP; Protein Data Bank code 1FKJ) (49) and to macrophage infectivity pro-

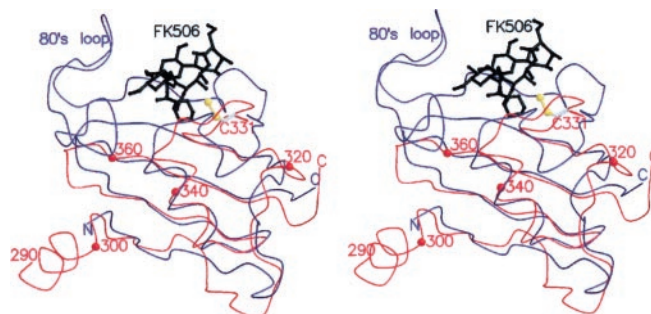


FIG. 4. Stereo view of the *LmMST* C-terminal domain superimposed onto the catalytic domain of FKBP (Protein Data Bank code 1FKJ). *LmMST* is shown in red, and FKBP in blue. C- α atoms of *LmMST* are numbered. The positions of Cys-331 in *LmMST* and the inhibitor FK506 (black sticks) bound to FKBP are also shown.

teinator protein (MIP; Protein Data Bank code 1FD9) (50). Comparison with FKBP revealed a sequence identity of 10%, and an overlay of 67 C- α pairs produced an r.m.s.d. of 2.3 Å and a Z-score of 6.0. In the case of MIP, the sequence identity is 12%, and the r.m.s.d. is 3.0 Å for 74 C- α pairs with a Z-score 5.7. FKBP is a peptidylprolyl *cis/trans*-isomerase (PPIase) class of immunophilin implicated in regulation of the mammalian immune response and basic cellular processes such as protein folding and trafficking (51). PPIases are often tightly associated with other proteins or are clearly distinguishable domains in larger polypeptides (52); and, in the case of *LmMST*, there is a distinct PPIase-like domain attached to a sulfurtransferase. MIP, a virulence factor implicated in host cell invasion, also displays PPIase activity and is found in bacteria such as *Legionella pneumophila* (50) and also in the trypanosomatid *Trypanosoma cruzi* (53).

The active site for the PPIase fold is a shallow pocket into which the inhibitor FK506 binds to form a complex that is a potent agonist of immunosuppression, exerting its effects through inhibition of the phosphatase activity of calcineurin (54). Superposition of the FKBP-FK506 complex onto the C-terminal domain of *LmMST* (Fig. 4) shows that the PPIase active site maps to a depression on the C-terminal domain of *LmMST* where the persulfurated Cys-331 is located. FK506 is included in Fig. 4 to highlight the position of Cys-331 within this potential ligand-binding pocket in the C-terminal domain of *LmMST*. In contrast to *LmMST*, the FKBP structure possesses extended loops and strands around the active-site pocket, including one formed by Thr-85 to Asn-94 and termed the “80s loop.” This loop acts as a flap to regulate access to the pocket (49, 54). Although lacking the extended loop structures, the altered position of the loop linking strand β 15 with helix α 11 (residues 330–335) of *LmMST* compared with that of FKBP places the side chains of Cys-331, Arg-333, Asp-335, and Arg-359 to interact with any potential ligands at this site (Fig. 5). Two salt bridges formed between Asp-335 and Arg-359 and between Glu-337 and Arg-359 are also present in the pocket, creating a distinct conformation that accommodates Cys-331 at one end (data not shown).

Assays for PPIase activity were carried out as described by Fischer *et al.* (55) using the FKBP- and cyclophilin-specific substrates succinyl-Ala-Leu-Pro-Phe-*p*NA and succinyl-Ala-Ala-Pro-Phe-*p*NA, respectively, but no activity could be detected (data not shown). However, the observation that truncated versions of *LmMST* do not express as soluble proteins suggests that the C-terminal domain makes an important contribution in stabilizing the overall fold (27). In this context, it is intriguing that the domain displays a fold common to a class of proteins implicated in regulating folding processes and in protein-protein associations and has a reactive cysteine placed in

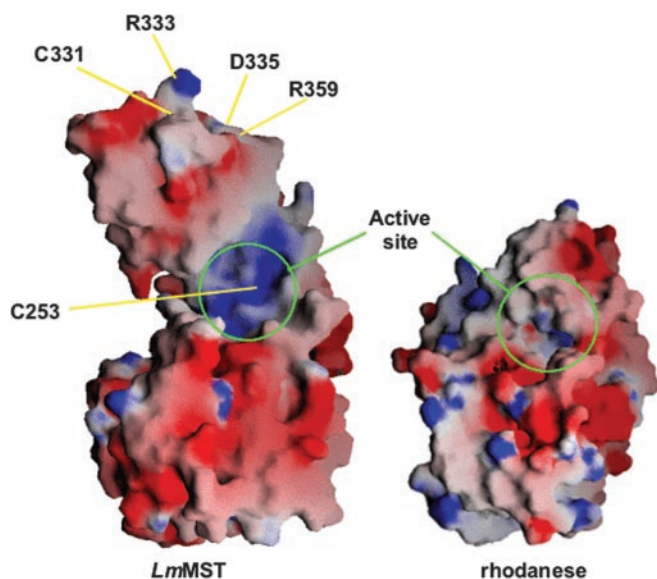


FIG. 5. Shape and surface charge representation of *LmMST* (left) and rhodanese (right) as calculated with the program GRASP (64). Blue denotes positive charge, and red denotes negative charge. The active sites of both *LmMST* and rhodanese are encircled in green, and the positions of residues in the C-terminal domain of *LmMST* that are discussed under “Results and Discussion” are marked.

the FKBP-like target-binding site. Further experiments will be required to determine how this domain contributes to the function of *LmMST*.

The MST Active Site—The active site is positioned in a cleft between the N-terminal and central domains (Fig. 2a) and is constructed from seven segments of the polypeptide. Five of these segments (residues 35–39, 72–75, 104–109, 193–196, and 253–258) are short loops between an α -helix and a β -strand; one is helix $\alpha 6$ (residues 180–185); and the longest stretch of polypeptide contributing directly to the active site (residues 209–221) encompasses $\theta 3$, $\beta 10$, and the loop leading into strand $\beta 11$.

The floor of the active site is formed mainly by the loop between strand $\beta 12$ and helix $\alpha 8$. Placed at the center of the loop is the side chain of the catalytic Cys-253, which is in the intermediate sulfur-substituted persulfide-containing state (Fig. 6). The conformation of the loop results in six amide groups from residues 254 to 259 placed to donate hydrogen bonds in toward the persulfide. On either side of the persulfide are the polar side chains of Ser-255 and Thr-258, the latter of which participates in a hydrogen bond with the persulfide S- δ . The “ring of persulfide-stabilizing NH groups” is similar to that observed in rhodanese (17). A further similarity to rhodanese is that the side chain of Cys-253 is likely influenced by dipoles from helices $\alpha 8$ and $\alpha 9$ of the central domain (Fig. 2a). The pK_a of the active site sulfhydryl group of rhodanese is low (~ 6.5) (56), probably because of contributions from the two-helix dipole, as discussed by Hol (57). In both *LmMST* and rhodanese, this dipole effect might enhance the reactivity of the active-site cysteine.

One side of the active-site cleft displays a basic patch formed by Arg-74, His-75, Arg-181, and Arg-185. Almost directly opposite is a hydrophobic area formed by a side-on contribution from Tyr-35 and the side chains of Leu-37, Met-108, and Val-257. Above this hydrophobic area, on the periphery of the active-site cleft, lie Glu-104 and Tyr-210. There are numerous hydrogen bonding interactions involving the amino acid side chains in and around the active site, which contribute to the structure of the cleft and placement of important functional groups. The interactions involving the catalytic Cys-253 have

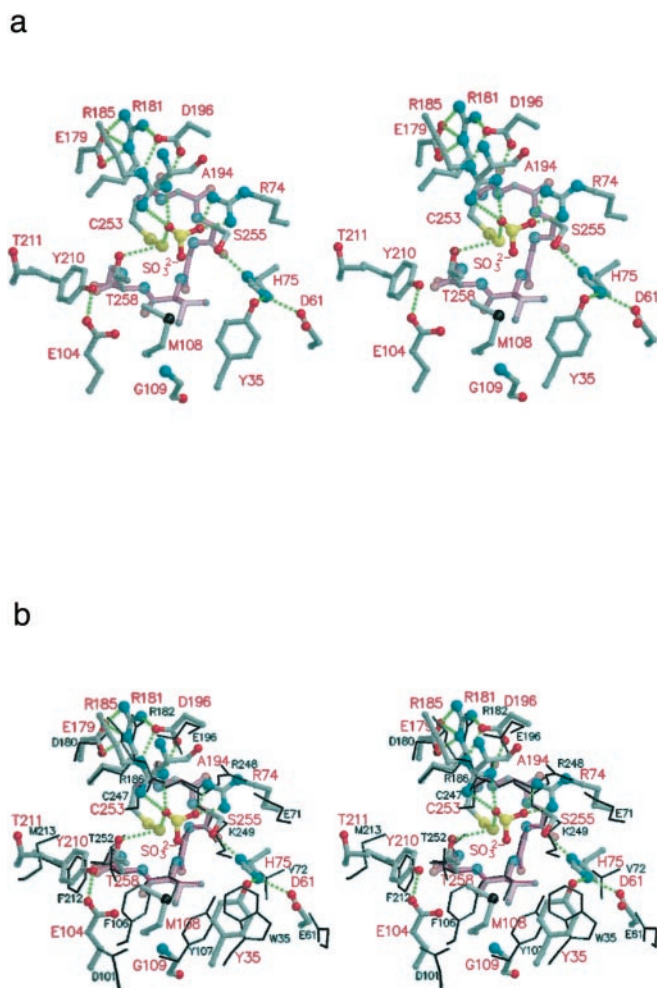


FIG. 6. Stereo view of the *LmMST* active site. *a*, the protein atoms are shown in a similar fashion to Fig. 1, with the exception that the active-site hexapeptide segment has the main chain bonds colored magenta, and the selenium of SeMet-108 is depicted as a black sphere. The dotted green lines represent possible hydrogen bonds, but such interactions between the persulfide sulfur and backbone amides have been omitted for clarity. *b*, an overlay with the selected side chains of bovine rhodanese shown as black sticks is presented.

already been described. Other associations of note are the interactions between Tyr-210 and Glu-104, His-75 and Tyr-35, and Asp-61 and Ser-255 (see below); Asp-179 and Asp-196 both interact with Arg-181, and Asp-196 also interacts with Arg-185. The guanidinium group of Arg-74 is the only polar side chain component lacking an interaction with some other functional group of the enzyme. This arginine, in conjunction with Arg-185, provides electrostatic interactions to bind a well ordered sulfite ion in the active site. The sulfite would prevent access to the catalytic center and is actually a potent inhibitor of rhodanese (15). A crystallographic study showed that metal cyanides bind at the entrance to the rhodanese active site in a similar fashion to the sulfite, thereby suggesting a common mechanism of action (58).

As mentioned above, a noteworthy difference between MSTs and rhodanases occurs in the active-site consensus sequence. Now that structures are available for both types of enzyme, we can describe the structural consequences of such differences; and, for comparative purposes, an overlay of the *LmMST* and bovine rhodanese active sites is presented in Fig. 6. This overlay identifies a number of structural features that are conserved in the active sites of the two enzymes. These include the loop that forms the floor of the active site and also a number of

hydrophobic and acidic residues that line one side of the cleft. In *LmMST*, Tyr-35, Met-108, and Tyr-210 are equivalent to and overlay well with Trp-35, Phe-106, and Phe-212 of rhodanese. Near to the hydrophobic patch in *LmMST* are Asp-61 and Glu-104, which are equivalent to Glu-61 and Asp-101 in rhodanese. Opposite the hydrophobic patch toward the sulfite-binding site is a highly conserved area of structure that, in *LmMST*, consists of Arg-181 and Arg-185 clustered with Glu-179 and Asp-196. In rhodanese, the equivalent residues are Arg-183, Arg-186, Asp-180, and Glu-196. A network of hydrogen bonding interactions involving these residues serves to place one of the arginines (*LmMST* Arg-185 or rhodanese Arg-186) to interact with ligands.

There are significant amino acid differences between the *LmMST* and rhodanese active sites that warrant discussion. Arg-74, His-75, Gly-109, Gly-254, and Ser-255 in *LmMST* are replaced by Glu-71, Val-72, Tyr-107, Arg-248, and Lys-249, respectively in bovine rhodanese. The Gly-109/Tyr-107 and Ser-255/Lys-249 differences reduce the size of the active-site cleft on one side, which is partially compensated for by the His-75/Val-72 difference. Three changes are relevant to differences in the active-site hexapeptide motif. To recap, in rhodanese, the consensus sequence is Cys-Arg-Lys-Gly-Val-Thr, and Arg-248 and Lys-249 change to Gly-254 and Ser-255 in *LmMST*. In rhodanese, Arg-248 interacts with Glu-71. In *LmMST*, Arg-74 is the equivalent of Glu-71 and occupies the space that is filled by Arg-248 in rhodanese and thereby compensates for the Gly-254/Arg-248 difference. The replacement of Arg-248 and Lys-249 of bovine liver rhodanese with glycine and serine, respectively, by site-directed mutagenesis decreases the TST activity and increases the MST activity, showing that these two amino acid positions are critical determinants of rhodanese/MST activity (6).

A molecular model of 3-mercaptopyruvate in the *LmMST* active site (data not shown), constructed on the basis that the carboxylate oxygen atoms would bind in the same position as the sulfite oxygen atoms, suggests that Arg-74 and Arg-185 are well placed to interact with the substrate. Indeed, the alteration of Arg-187 in rat liver MST (the equivalent of Arg-185 in *LmMST*) reduces binding of 3-mercaptopyruvate significantly (24). Mutation of *LmMST* Arg-74 might have a similar effect.

Ser-255 could contribute to the binding of 3-mercaptopyruvate by interaction with the carbonyl group. Such an interaction could polarize the carbonyl group and serve to enhance nucleophilic attack by the Cys-253 thiolate, allowing the enzyme to then attain the persulfide form by turnover of the appropriate sulfur donor. Ser-255 in *LmMST* is equivalent to Lys-249 in rhodanese, a residue that directly interacts with thiosulfate. Significantly, alteration by site-directed mutagenesis of the equivalent serine in rat liver MST (Ser-249) (24) or in *E. coli* SseA (Ser-240) (25) to lysine directs specificity away from 3-mercaptopyruvate toward thiosulfate.

Both *LmMST* and rhodanese active sites are positively charged (Fig. 5) to attract and then bind negatively charged ligands. The active-site cleft and immediate vicinity of *LmMST* are positively charged because of the basic patch described above and contributions from Lys-38, Lys-40, and Lys-197 together with Arg-289. These last four residues are not conserved in rhodanese, which in part explains why the TST active site appears less positively charged. It seems likely that the electrostatic properties of physiological substrates would complement those of the individual sulfurtransferases.

A Serine Protease-like Triad—Two residues, His-75 and Ser-255 (discussed above in the context of differences between MSTs and bovine rhodanese), in conjunction with Asp-61, are arranged in a serine protease-like triad at the active site (Fig.

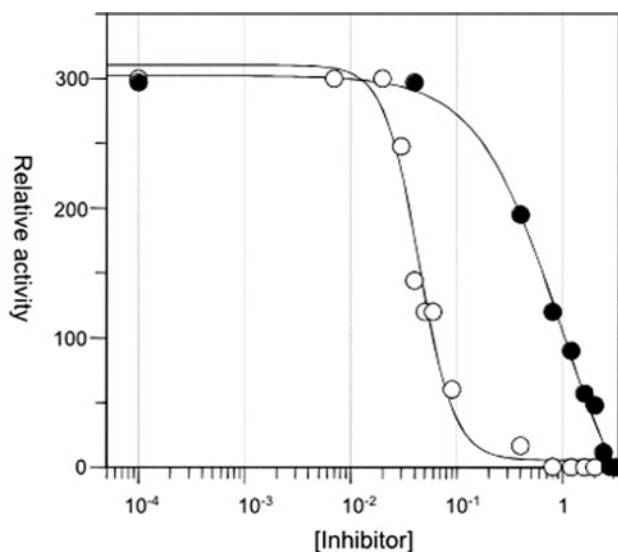


FIG. 7. Effect of serine peptidase inhibitors on sulfurtransferase activity. *LmMST* (0.09 $\mu\text{g/ml}$) was preincubated for 30 min at 37 $^{\circ}\text{C}$ in 100 mM Tris-HCl (pH 8.0) containing varying concentrations (mM) of phenylmethanesulfonyl fluoride (○) and TLCK (●). The residual activity was measured at 37 $^{\circ}\text{C}$ with 5 mM mercaptopyruvate and 5 mM mercaptoethanol buffered in 100 mM Tris-HCl (pH 8.0).

6). The distance between Ser-255 O- γ and His-75 N- δ 1 is 2.9 \AA , and that between His-75 N- ϵ 2 and Asp-61 O- δ 1 is 2.8 \AA . His-75 participates in a three-center hydrogen bond with Asp-61 and the hydroxyl group of Tyr-35 (3.0 \AA distant). The triad is aligned perpendicular to the active-site entrance at the surface of the enzyme. Sequence alignments (discussed above) indicate that this triad is a common and, we predict, defining feature of the MST family, distinguishing MSTs from TSTs. Ser-255 and His-75 are strictly conserved, whereas Asp-61 is more variable, present as glutamate or asparagine. TST family members retain the aspartate/glutamate equivalents, but lack the histidine and serine equivalents.

As a result of the structure determination of *LmMST* and our sequence-structure analysis, we now know that the characteristic combination of an acidic residue, a histidine, and a serine that form a serine protease-like triad is conserved in the MST sequences and therefore can be used as an extension of the Cys-Gly-Ser-Gly-Val-(Thr/Ser) motif to identify members of the MST family of enzymes. The triad presumably exists as a means of activating the serine for its role in binding and polarizing the carbonyl group of 3-mercaptopyruvate to assist thiophilic attack.

Is *LmMST* a Protease?—Once a serine protease-like Asp-His-Ser triad was noted, we decided to investigate whether *LmMST* does indeed display protease activity and whether classical serine protease inhibitors affect the protein. Peptidyl-pNA substrates with arginine at the P₁ position were used to test for protease activity. In the presence of β -mercaptoethanol, *LmMST* hydrolyzed Bz-Arg-pNA, albeit at a low rate (3.6 nmol/min/mg of protein) relative to the control enzyme trypsin (150 $\mu\text{mol/min/mg}$ of protein). Peptidyl substrates with phenylalanine and valine or with proline and phenylalanine occupying the P₃ and P₂ positions, respectively, were also hydrolyzed, but at a rate \sim 50% of that observed for Bz-Arg-pNA, whereas Bz-Arg-Arg-pNA was not hydrolyzed at all. All activities were inhibited by 0.5 mM TLCK. TLCK and phenylmethanesulfonyl fluoride, known inhibitors of trypsin-like serine proteases, also effectively inhibited the sulfurtransferase activity of *LmMST*, with IC₅₀ values of 44 and 700 μM , respectively (Fig. 7). In contrast, TPCK, an inhibitor of chymotrypsin-like serine proteases, and E-64, an inhibitor of cysteine proteases, had no

effect on *LmMST* within the ranges of inhibitors tested. These results indicate that Ser-255 is activated, which is consistent with its orientation within the triad; and this accounts for the enzyme's low level of serine protease activity and the susceptibility of the enzyme to inhibition by TLCK and phenylmethanesulfonyl fluoride. Binding of these molecules would affect both access of the substrate to the active site, through steric hindrance, and the part played by the activated serine in polarizing the carbonyl group of the substrate as part of the catalytic process. A higher level of protease activity could exist with a physiological substrate, but it is perhaps more likely that the triad primarily serves to position the serine hydroxyl group to bind and polarize substrate during the reaction

Concluding Remarks—With this high resolution crystal structure determination of *LmMST*, we now have accurate models for the two distinctive subclasses of sulfurtransferases. This, in conjunction with biochemical analyses, has provided important insights into the structure-activity relationships for a widely distributed enzyme. Most interestingly, it has been shown that MSTs contain a serine protease-like catalytic triad in their active site. Although such triads exist in esterases and lipases, this is the first demonstration that such a distinctive structural feature also occurs in some sulfurtransferases.

The analysis provides information on how TST and MST differ and also on how they are adapted to interact with and process different substrates. Understanding the significance of these differences in terms of physiological functions of the enzymes is hindered by the limited information available about the biological roles of the distinct sulfurtransferases. A contributing factor to this problem may be the diverse roles that this widely distributed class of enzymes can play. Nevertheless, a picture is starting to emerge of an enzyme activity that is up-regulated in response to stress. Rhodanese and proteins containing rhodanese-like domains are implicated in response to heat shock, phage shock, and senescence (13, 23). MSTs have been implicated in the management of oxidative stress (27, 28), and the trypanosomatid *LmMST* is also linked to cysteine biosynthesis (27). It is noteworthy that the trypanothione peroxidase pathway, so critical to the regulation of oxidative stress in trypanosomatids, consists of four components: three proteins (trypanothione reductase, tryparedoxin, and tryparedoxin peroxidase) and the polyamine peptide metabolite trypanothione (59, 60). All four components are critically dependent on the redox properties of cysteine pairs (61).

The structure of *LmMST* has also revealed a peculiarity of the trypanosomatid MSTs. They contain a domain that is structurally homologous to a type of PPIase molecular chaperone. PPIase domains that are components of larger proteins have been reported previously, although this is the first example that combines a PPIase-like domain with rhodanese domains, which, in addition, also contain a protease-like catalytic triad. Interestingly, it has been reported recently that *E. coli* Hsp31, a type of heat shock protein, combines a chaperone function, although not using a PPIase-type of fold, with a structure that also displays a catalytic triad, this time a cysteine protease-like triad (62). The *E. coli* Hsp31 protein functions both as a sensor to monitor the correct folding of polypeptides and as a protease to degrade those that are misfolded. It may be instructive to explore similar roles for selected sulfurtransferases

Acknowledgments—We thank Kenneth Beattie (Post-Genomics and Molecular Interactions Centre) for mass spectrometry, Charles Bond for discussions, Gordon Leonard (European Synchrotron Radiation Facility) for advice and support at the synchrotron, Sylvain Eschenlauer for help with the PPIase assays, and the European Synchrotron Radiation Facility for access.

REFERENCES

- Bordo, D., and Bork, P. (2002) *EMBO Rep.* **3**, 741–746
- Nakamura, T., Yamaguchi, Y., and Sano, H. (2000) *Eur. J. Biochem.* **267**, 5621–5630
- Papenbrock, J., and Schmidt, A. (2000) *Eur. J. Biochem.* **267**, 145–154
- Ogata, K., and Volini, M. (1990) *J. Biol. Chem.* **265**, 8087–8093
- Pagani, S., Bonomi, F., and Cerletti, P. (1984) *Eur. J. Biochem.* **142**, 361–366
- Nagahara, N., Ito, T., and Minami, M. (1999) *Histol. Histopathol.* **14**, 1277–1286
- Sorbo, B. H. (1957) *Biochim. Biophys. Acta* **24**, 324–329
- Hannestad, U., Martensson, J., Sjødahl, R., and Sorbo, B. (1981) *Biochem. Med.* **26**, 106–114
- Nishino, T., Usami, C., and Tsushima, K. (1983) *Proc. Natl. Acad. Sci. U. S. A.* **80**, 1826–1829
- Ogasawara, Y., Lacourciere, G., and Stadtman, T. C. (2001) *Proc. Natl. Acad. Sci. U. S. A.* **98**, 9494–9498
- Mueller, E. G., Palenchar, P. M., and Buck, C. J. (2001) *J. Biol. Chem.* **276**, 33588–33595
- Palenchar, P. M., Buck, C. J., Cheng, H., Larson, T. J., and Mueller, E. G. (2000) *J. Biol. Chem.* **275**, 8283–8286
- Adams, H., Teertstra, W., Koster, M., and Tommassen, J. (2002) *FEBS Lett.* **518**, 173–176
- Meister, A. (1953) *Fed. Proc.* **12**, 245
- Gliubich, F., Berni, R., Colapietro, M., Barba, L., and Zanotti, G. (1998) *Acta Crystallogr. Sect. D* **54**, 481–486
- Gliubich, F., Gazerro, M., Zanotti, G., Delbono, S., Bombieri, G., and Berni, R. (1996) *J. Biol. Chem.* **271**, 21054–21061
- Hol, W. G., Lijk, L. J., and Kalk, K. H. (1983) *Fundam. Appl. Toxicol.* **3**, 370–376
- Ploegman, J. H., Drent, G., Kalk, K. H., and Hol, W. G. (1978a) *J. Mol. Biol.* **123**, 557–594
- Ploegman, J. H., Drent, G., Kalk, K. H., and Hol, W. G. (1979) *J. Mol. Biol.* **127**, 149–162
- Ploegman, J. H., Drent, G., Kalk, K. H., Hol, W. G., Heinrikson, R. L., Keim, P., Weng, L., and Russell, J. (1978) *Nature* **273**, 124–129
- Spallarossa, A., Donahue, J. L., Larson, T. J., Bolognesi, M., and Bordo, D. (2001) *Structure* **9**, 1117–1125
- Fauman, E. B., Cogswell, J. P., Lovejoy, B., Rocque, W. J., Holmes, W., Montana, V. G., Piwnica-Worms, H., Rink, M. J., and Saper, M. A. (1998) *Cell* **93**, 617–625
- Hofmann, K., Bucher, P., and Kajava, A. V. (1998) *J. Mol. Biol.* **282**, 195–208
- Nagahara, N., Okazaki, T., and Nishino, T. (1995) *J. Biol. Chem.* **270**, 16230–16235
- Nagahara, N., and Nishino, T. (1996) *J. Biol. Chem.* **271**, 27395–27401
- Colnaghi, R., Cassinelli, G., Drummond, M., Forlani, F., and Pagani, S. (2001) *FEBS Lett.* **500**, 153–156
- Williams, R. A. M., Kelly, S. M., Mottram, J. C., and Coombs, G. H. (2003) *J. Biol. Chem.* **278**, 1480–1486
- Nandi, D. L., and Westley, J. (1998) *Int. J. Biochem. Cell Biol.* **30**, 973–977
- Nandi, D. L., Horowitz, P. M., and Westley, J. (2000) *Int. J. Biochem. Cell Biol.* **32**, 465–473
- Ray, W. K., Zeng, G., Potters, M. B., Mansuri, A. M., and Larson, T. J. (2000) *J. Bacteriol.* **182**, 2277–2284
- Mendoza, J. A., Rogers, E., Lorimer, G. H., and Horowitz, P. M. (1991) *J. Biol. Chem.* **266**, 13044–13049
- Jancarik, J., and Kim, S.-H. (1991) *J. Appl. Crystallogr.* **24**, 409–411
- Otwinowski, Z., and Minor, W. (1996) *Methods Enzymol.* **276**, 307–326
- Terwilliger, T. C., and Berendzen, J. (1999) *Acta Crystallogr. Sect. D* **55**, 849–861
- Otwinowski, Z. (1991) in *Isomorphous Replacement and Anomalous Scattering* (Leslie, A. G. W., ed) pp. 80–86, Science and Engineering Research Council, Daresbury Laboratory, Warrington, United Kingdom
- Cowtan, K. (1994) *Joint CCP4 ESF-EACBM Newsletter* **31**, 34–38
- Perrakis, A., Sixma, T. K., Wilson, K. S., and Lamzin, V. S. (1997) *Acta Crystallogr. Sect. D* **30**, 551–554
- Levitt, D. G. (2001) *Acta Crystallogr. Sect. D* **57**, 1013–1019
- Vagin, A., and Teplyakov, A. (1997) *J. Appl. Crystallogr.* **30**, 1022–1025
- Jones, T. A., Zou, J. Y., Cowan, S. W., and Kjeldgaard, M. (1991) *Acta Crystallogr.* **40**, 110–119
- Brünger, A. T. (1993) *Acta Crystallogr. Sect. D* **49**, 24–36
- Brünger, A. T., Adams, P. D., Clore, G. M., DeLano, W. L., Gros, P., Grosse-Kunstleve, R. W., Jiang, J. S., Kuszewski, J., Nilges, M., Pannu, N. S., Read, R. J., Rice, L. M., Simonson, T., and Warren, G. L. (1998) *Acta Crystallogr. Sect. D* **54**, 905–921
- Murshodov, G. N., Vagin, A. A., and Dodson, E. J. (1997) *Acta Crystallogr. Sect. D* **53**, 240–255
- Laskowski, R. A., MacArthur, M. W., Moss, D. S., and Thornton, J. M. (1995) *J. Appl. Crystallogr.* **26**, 283–291
- Hutchinson, E. G., and Thornton, J. M. (1996) *Protein Sci.* **5**, 212–220
- Thomson, J. D., Higgins, D. G., and Gibson, T. J. (1994) *Nucleic Acids Res.* **22**, 4673–4680
- Holm, L., and Sander, C. (1993) *J. Mol. Biol.* **233**, 123–138
- Berman, H. M., Westbrook, J., Feng, Z., Gilliland, G., Bhat, T. N., Weissig, H., Shindyalov, I. N., and Bourne, P. E. (2000) *Nucleic Acids Res.* **28**, 235–242
- Wilson, K. P., Yamashita, M. M., Sintchak, M. D., Rotstein, S. H., Murcko, M. A., Boger, J., Thomson, J. A., Fitzgibbon, M. J., Black, J. R., and Navia, M. A. (1995) *Acta Crystallogr. Sect. D* **51**, 511–521
- Riboldi-Tunnicliffe, A., König, B., Jessen, S., Weiss, M. S., Rahfeld, J., Hacker, J., Fischer, G., and Hilgenfeld, R. (2001) *Nat. Struct. Biol.* **8**, 779–783
- Fischer, G. (1994) *Angew. Chem. Int. Ed. Engl.* **33**, 1415–1436
- Kamphausen, T., Fanghänel, J., Neumann, D., Schulz, and Rahfeld, J. (2002) *Plant J.* **32**, 263–276

53. Pereira, P. J., Vega, M. C., González-Rey, E., Fernandez-Carazo, R., Macedo-Ribreiro, S., Gomis-Rüth, F. X., González, A., and Coll, M. (2002) *EMBO Rep.* **3**, 94–99
54. Sinars, C. R., Cheung-Flynn, J., Rimerman, R. A., Scammell, J. G., Smith, D. F., and Clardy, J. (2003) *Proc. Natl. Acad. Sci. U. S. A.* **100**, 868–873
55. Fischer, G., Wittmannlied, B., Lang, K., Kiefhaber, T., and Schmid, F. X. (1989) *Nature* **337**, 476–478
56. Schlesinger, P., and Westley, J. (1974) *J. Biol. Chem.* **249**, 780–788
57. Hol, W. G. (1985) *Prog. Biophys. Mol. Biol.* **45**, 149–195
58. Likj, L. J., Kalk, K. H., Brandenburg, N. P., and Hol, W. G. J. (1983) *Biochemistry* **22**, 2952–2957
59. Fairlamb, A. H., and Cerami, A. (1992) *Annu. Rev. Microbiol.* **46**, 695–729
60. Krauth-Siegel, R. L., and Coombs, G. H. (1999) *Parasitol. Today* **15**, 404–409
61. Alphey, M. S., Bond, C. S., Tetaud, E., Fairlamb, A. H., and Hunter, W. N. (2000) *J. Mol. Biol.* **300**, 903–916
62. Quigley, P. M., Korotkov, K., Baneyx, F., and Hol, W. G. (2003) *Proc. Natl. Acad. Sci. U. S. A.* **100**, 3137–3142
63. Kraulis, P. J. (1991) *J. Appl. Crystallogr.* **24**, 946–950
64. Nicholls, A. (1993) *GRASP Manual*, Version 1.1, Columbia University, New York